Droplet Formation and Impingement Dynamics of Low-Boiling Refrigerant on Solid Surfaces with Different Roughness under Atmospheric Pressure

Shu-Yan Chen [1], Dong-Qing Zhu [1], Hong-Jie Xing [1], Qin Zhao [2,3], Zhi-Fu Zhou [1,*] and Bin Chen [1]

1   State Key Laboratory of Multiphase Flow in Power Engineering, Xi'an Jiaotong University, Xi'an 710049, China
2   College of Mechanical and Vehicle Engineering, Chongqing University, Shazhengjie No. 174, Chongqing 400044, China
3   State Key Laboratory of Vehicle NVH and Safety Technology, Chongqing 401122, China
*   Correspondence: zfzhou@mail.xjtu.edu.cn

Abstract: The dynamic behavior of droplet impingement is one of the most important processes of spray cooling. Although refrigerants with a low boiling point have been widely used in spray cooling, their high volatility makes it difficult to generate a stable droplet under atmospheric pressure, and thus the dynamic behavior of droplet impingement is rarely reported. Therefore, it is of great significance to study the behavior of refrigerant droplet impingement to fill the relevant research gaps. In this paper, an experimental system for single refrigerant droplet generation and impingement at atmospheric pressure has been established. By means of high-speed photography technology, the morphology and dynamics of R1336mzz(Z) droplet impingement on grooved carbon steel walls have been studied. Phenomena such as a truncated sphere, boiling, and finger-shaped disturbance were observed, and the reasons responsible for them were analyzed. The effects of Weber number (We) and surface roughness (Ra) on droplet spreading factor (β) were investigated quantitatively. Higher We always causes a larger β_{max}, while Ra has a different influence on β_{max}. The Cassie–Wenzel transition occurs when Ra increases from 1.6 μm to 3.2 μm, leading to a rapid decrease in β_{max}. An empirical formula has been proposed to predict β_{max} under different conditions.

Keywords: R1336mzz(Z) droplet; surface roughness; morphological characteristics; spreading factor; spray cooling

1. Introduction

Spray cooling has the advantages of strong heat dissipation, low required flow rate, and high heat transfer coefficient [1–3]. It has been widely applied in the heat dissipation of photovoltaic cells [4], high-power electronic chips [5,6], laser treatment for port wine stains [7,8], and so on. It is relatively difficult to observe the micro-dynamic behavior and study the thermal and kinetic mechanisms during spray impingement because of the complex interactions between numerous droplets with cooling surfaces and between droplets themselves. Therefore, researchers pay more attention to the impact behavior of a single droplet. On the one hand, single droplet behavior, including impinging dynamics and heat and mass transfer, is one of the most important processes during spray impingement. On the other hand, single droplet impingement simplifies the process of investigating the fundamentals of spray cooling in a controllable system and offers the ability to investigate the influence of different parameters in isolation.

Early in 1876, Worthington et al. [9] studied the morphology of water and mercury droplets impacting a solid surface or liquid with a certain depth, initiating the study of droplet impingement. Scholars have carried out numerous studies on morphology evolution and the heat and mass transfer process of droplet impingement. In the past

20 years, with the development of high-speed photography technology, the observation of droplet impact has made further progress. When droplets impact solid walls, the outcomes are spreading, splash, rebound, partial rebound, deposition, retreat (recoil), ejection, and fingering [10]. Identifying different outcomes and developing corresponding transition criteria are important [11].

These behaviors are dependent on the characteristics of the droplet, surface, and ambient conditions. Some researchers have investigated droplet properties characterized by diameters, viscosity, surface tension, density, velocity, and temperature. Bhardwaj et al. [12] numerically investigated the impingement of heated water droplets at atmospheric pressure and suggested warm droplets spread more violently than cold droplets due to larger Re. Prathamesh et al. [13] investigated the effect of impact velocity and concluded that larger velocity resulted in larger spreading and amplitude of oscillation. Seo et al. [14] noted that few studies investigated low-viscosity droplets, while most studies explored droplet impingement using water and glycerin. An empirical model for predicting the maximum spreading diameter was proposed by analyzing the impingement of gasoline, isooctane, and ethanol droplets. Tian et al. [15] systematically investigated the effects of droplet diameter, impact velocity, viscosity, and surface tension on droplet impact dynamics using R113, deionized water, ethanol, and acetone. Large viscosity and surface tension were found to hinder droplet spreading, whereas the initial droplet diameter minimally affected the spreading factor. Moreover, Xu et al. [16] found that reduction of the ambient pressure could suppress the corona splash by investigating methanol, ethanol, and 2-propanol impingements. As for low-boiling refrigerants commonly used in cryogen spray cooling, they show obviously different characteristics, such as lower viscosity, lower surface tension, and high volatility. However, the impingement dynamics of a single droplet with a low boiling point and high volatility are rarely reported.

Surface conditions are characterized by temperature, roughness, wettability (i.e., hydrophilic or hydrophobic), and thermal conductivity. Range et al. [17] proposed that roughness was an important factor affecting the morphology of water droplet impingement on solid walls. Therefore, it is of great significance to study the influence of roughness on the dynamic behavior of droplet impingement. Tang et al. [18] studied high-boiling R113 droplet impingement as a replacement for low-boiling R134a because of the similar physical properties of R113 and R134a. It was found that a rough surface can reduce the splash threshold of a droplet, and surface roughness was considered in the empirical formula of maximum spread diameter. Kuhn et al. [19] studied droplet impingement of urea water solution on heated porous surfaces. The effects of substrate roughness on the splash, evolution process, and heat transfer were discussed. More recently, the dynamic behaviors of droplet impact on groove-textured surfaces have attracted a lot of interest because of its anisotropy in wettability [20]. Vaikuntanathan et al. [21] proposed that the pinning force exerted by the surface roughness on the three-phase contact line at the periphery did negative work and hindered the droplet spreading due to the energy consumed by the droplet's penetration into the groove-textured structures. They also proposed models of the maximum spreading diameter based on energy conservation. Minhee et al. [22] obtained different kinds of disturbances with radioactive strips on the surface during deionized water droplet impingement. Moon et al. [23] analyzed the characteristic of dynamic contact angle on textured surfaces influenced by texture area fraction, Weber number, and surface temperature. Ogata Satoshi et al. [24] designed a low-cost, layered texture surface of heated walls to improve the Leidenfrost Point (LFP) of deionized water on a nanocoated mesh surface. Lv et al. [25] studied droplet dynamics impinging on superhydrophobic surfaces, revealing that the contact time was determined by the Weber number and surface roughness. Further, Zhang et al. [26] from the same research group investigated droplet impact dynamics on superhydrophobic surfaces with submillimeter-scale posts, in which an intriguing droplet breakup mechanism of internal rupture was found. This type of breakup greatly shortened the contact time up to 50% compared with the traditional rebound and rim breakup mechanism.

In general, scholars have carried out numerous studies on the impact behavior of water, ethanol, and other relatively high boiling-point droplets with low volatility. Though low-boiling refrigerants have been widely used in the field of spray cooling, their high volatility makes it difficult to control and generate a stable droplet at normal atmospheric pressure. There are few reports on the experimental study of the impinging dynamics for single refrigerant droplets, leaving related research and simulation calculations short of reliable data reference. Therefore, establishing a droplet formation system and studying the morphology and dynamic characteristics of low-boiling refrigerant droplet impingement are of vital importance. There are two options to study cryogen droplet impingement. One is to generate a cryogen droplet in a high-pressure environment because high pressure reduces droplet volatility and, thus, could keep the cryogen as a stable droplet before impingement. Liu et al. [27–29] studied R134a droplet impact on a solid surface in a visual high-pressure vessel and proposed a model to accurately predict the maximum spreading diameter with a large range of surface roughness. However, the high-pressure environment makes it difficult to observe the impact behavior, and the high-pressure vessel has the potential risk of explosion. This study adopted an alternative to cool the cryogen under dew-point temperature at atmospheric pressure before its discharge. This approach can generate a stable cryogen droplet under the atmospheric environment without the high-pressure vessel. Thus, it is far easier and safer to conduct the experiment. Moreover, different from those at high pressure, the liquid properties and air–liquid interaction that affected the impact results conformed with most of the application scenarios at atmospheric pressure.

The selection of refrigerant should conform to working conditions such as different temperatures, pressure, thermal stability, and so on. At the same time, the refrigerant should be environmentally friendly. The refrigerant R1336mzz(Z) is considered a competitive working fluid in flashing spray cooling systems to achieve effective heat dissipation for high-power density chips [30] due to the advantages of low saturation temperature (33 °C under atmospheric pressure), zero ozone depleting potential (ODP = 0) and low global warming potential (GWP = 2) [31]. Zhang et al. [30] demonstrated that R1336mzz(Z) spray cooling could achieve a good heat transfer performance with CHF of 349 W/cm^2 under a surface temperature below 80 °C, which had great significance for the practical application of spray cooling in high-power density chips due to the safe working temperature. However, the behavior and mechanism of single droplet impingement of R1336mzz(Z) remain to be further explored.

In this paper, an experimental system to study low-boiling refrigerant droplet impingement has been built. It is able to preserve and generate a stable low-boiling refrigerant droplet under atmospheric pressure and record the droplet spreading process with a high-speed camera. The effects of Weber number and surface roughness on the morphology evolution and dynamic process of R1336mzz(Z) droplet impingement are comprehensively explored.

2. Experimental System and Measurement Methods

2.1. Experimental System

As shown in Figure 1, the experimental system was set on a level optical platform to guarantee vertical impingement. It includes a droplet generating system, a one-dimensional positioner, an image acquisition system, and solid surfaces. Among them, the droplet generating system includes an insulated tank with thermostatic water bath circulation and a detachable nozzle with an inner diameter of 2 mm. The temperature in the tank is monitored in real-time by thermocouples and a data acquisition system. The insulated tank moves in the vertical direction to change the impinging height of the droplet in free fall and droplet impingement velocity. The adjustment range of height is 0–50 cm. In the experiment, the backlight photography method was adopted, and the data were collected by an image acquisition system, including a background light source (LED), photoelectric sensor, computer, and a high-speed camera (FASTCAM SA-Z, Photron, Tokyo, Japan) with a shooting rate of 20,000 fps and a resolution of 1024 × 1024. In order to preserve the

R1336mzz(Z) in liquid and control the experimental variables as much as possible, the temperature of the water bath was controlled at 0 °C. The temperature of R1336mzz(Z) was maintained at 5 ± 1 °C accordingly, considering the heat dissipation of the tank and pipe. The properties of R1336mzz(Z) at 5 °C are listed in Table 1. The experiment was conducted at room temperature (20 ± 3 °C) and atmospheric pressure.
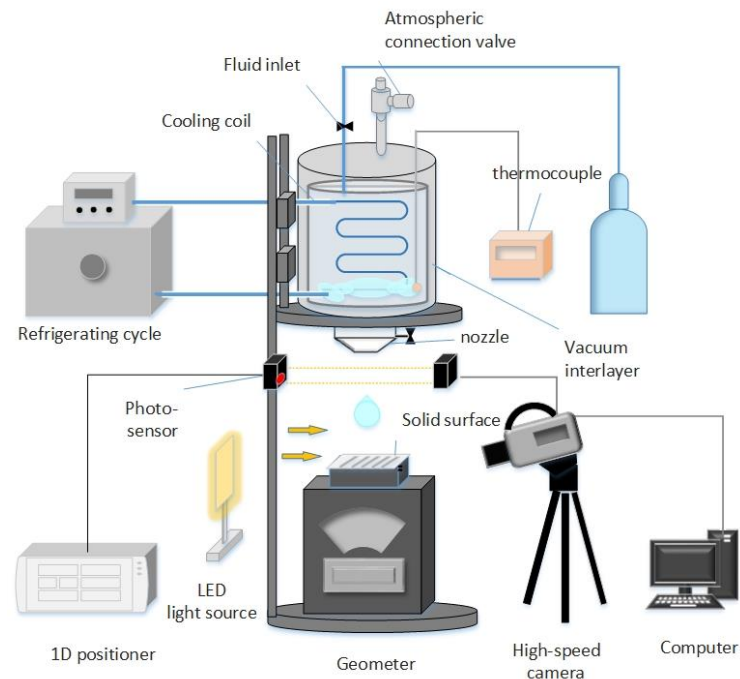

Figure 1. Schematic of the experimental system.

Table 1. Properties of R1336mzz(Z) (5 °C,1 atm).

Properties	R1336mzz(Z)
Surface tension σ (mN m^{-1}) [32]	14.35
Density ρ (kg m^{-3}) [32]	1428.07
Viscosity μ (μkg m^{-1} s^{-1}) [33]	493.04
Boiling point (°C) [31]	33
ODP [31]	0
GWP [31]	2

The experimental procedures are as follows. First, the refrigerating cycle is turned on to reduce the R1336mzz(Z) liquid temperature within the insulated tank to 5 °C. Afterward, a single droplet can be generated by gravity with no initial velocity once the nozzle valve is opened slowly. When the droplet freely falls to the area near the solid surface, it triggers the photoelectric sensor installed near the surface, and the signal from the photoelectric sensor triggers the high-speed camera to record the impacting images of the droplet. Each experiment was repeated twice to ensure repeatability.

To explore the influence of surface characteristics on droplet impingement, four standard reference specimens with different roughnesses made of carbon steel 45, namely groove textured surface, were selected for the experiment. The parameter *Ra* well represents the surface roughness, which is 0.8 μm, 1.6 μm, 3.2 μm, and 6.3 μm. The selection of roughness and droplet size in the experiment referenced the work done by Tang et al. [18].

Notably, nozzles were used to generate droplets. For the normal flat nozzle, droplets are more likely to attach to the plane surface before falling. This leads to a series of small droplets or liquid columns when the droplets fall, and the diameter of the generated droplets diverges greatly. In the process of experiments and observation, this paper changed the flat nozzle into a conical nozzle with an inner diameter of 2 mm, as shown in Figure 2.

The phenomenon of accompanied droplets was obviously improved. In addition, the divergence of the droplet diameter was apparently reduced, as shown in the picture. The theoretical value of drop diameter D_T can be calculated from the equilibrium of the gravity and the capillary force acting between the nozzle and the droplet [34]:

$$D_T = \left(\frac{6D_{in}\sigma}{\rho g}\right)^{1/3} \tag{1}$$

where σ is the surface tension of liquid, D_{in} is the nozzle inner diameter, ρ is the droplet density, and g is the gravity constant. The theoretical value of the droplet is calculated as 2.309 mm by the formula. The droplet diameter distribution generated from the improved nozzle is concentrated, and the error is within 10% compared with the theoretical value, as shown in Figure 2. Analysis in the following section adopts the experimental value of droplet size measured in pictures.
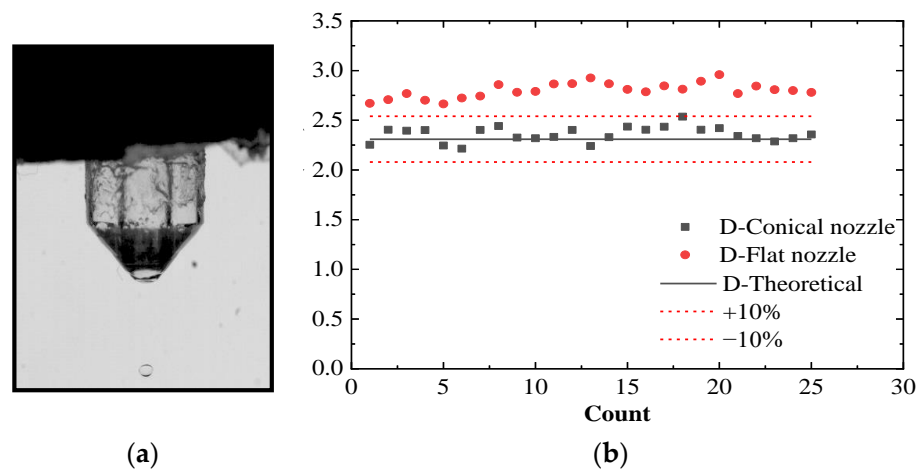

Figure 2. Image of (**a**) conical nozzle and (**b**) comparison of droplet diameter distributions resulting from the flat and conical nozzles.

2.2. Parameters

To evaluate the dynamic behavior of droplets and qualitatively analyze the morphological changes of droplets, several nondimensionalized factors are adopted to characterize the droplet behavior. Spreading factor, calculated by $\beta = D/D_0$, is a key parameter to evaluate the dynamic behavior of droplets, representing the ability of droplet spreading, where D is the spreading diameter of droplets after impact, and D_0 is the initial diameter of the droplet before impact. A dimensionless spreading time $\tau = \frac{tV_0}{D_0}$ is also employed, where t is the time duration of the droplet impacting process. The impacting velocity is calculated by using the equation [17]:

$$V_0 = \sqrt{\frac{g}{A}\left(1 - \exp(2A(D_0 - H))\right)} \tag{2}$$

$$A = \frac{3}{4}\frac{\rho_{air}C_f}{\rho D_0} \tag{3}$$

where H is the falling height and Friction coefficient C_f in this formula is 0.796 according to Range and Feuillebois [17]. The equivalent initial diameter D_0 is calculated by $D_0 = \left(D_h^2 D_v\right)^{\frac{1}{3}}$ [15,35], as shown in Figure 3, because the droplet is not perfectly spherical, where D_h and D_v are diameters in horizontal and vertical directions. Three dimensionless numbers on droplet impinging dynamics are mainly studied: *We* represents the ratio of inertial force and liquid surface tension, *Re* represents the ratio of inertial force and viscous

force, and *Oh* represents the relationship between viscous force, inertial force, and surface tension. Their mathematical expressions are as follows:

$$We = \frac{\rho D_0 V_0^2}{\sigma} \tag{4}$$

$$Re = \frac{\rho D_0 V_0}{\mu} \tag{5}$$

$$Oh = \frac{\mu}{(\rho \sigma D_0)^{0.5}} \tag{6}$$

where ρ, σ, μ, D_0 and V_0 represent the density, surface tension, viscosity, initial diameter, and impact velocity of droplets, respectively. Dynamic parameters of droplets are obtained from images shot by a high-speed camera.
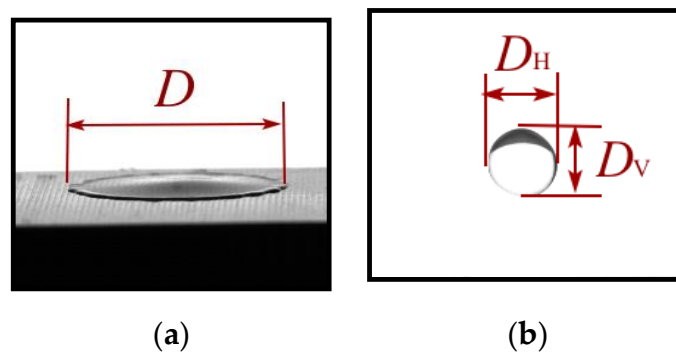

(**a**)   (**b**)

Figure 3. Parameters of droplet. (**a**) droplet spreading diameter. (**b**) droplet diameters in horizontal and vertical directions.

3. Results and Discussions

In this experiment, we studied the dynamic behavior of R1336mzz(Z) refrigerant droplets impacting surfaces with different roughness based on the refrigerant droplet generating system. The values of *Ra* for carbon steel surfaces were 0.8 μm, 1.6 μm, 3.2 μm, and 6.3 m. The range of falling height is 2–26 cm. The corresponding theoretical impacting velocity range is 0.584–2.189 m/s, and the *We* number studied is in the range of 50–1000.

3.1. The Influence of We

Firstly, we discuss the results of droplet morphology under three different *We* on the low-roughness surface (*Ra* = 0.8 μm as shown in Figure 4a–c) and high-roughness surface (*Ra* = 6.3 μm as shown in Figure 4d–f). Scale bars were labeled for each group of impacting images. As shown in Figure 4a for the low *We* number case (*We* = 77), the droplet deforms once it impacts the surface, forming a truncated spherical shape at first, and subsequently, a thin liquid layer is formed at the bottom of the droplet (0.60 ms). Then, the thin layer of liquid gradually spreads. Finally, the droplets spread to the maximum diameter (16.00 ms), forming a thin central part bordered by a thick cylindrical rim. The droplet front is pinned at the edge of solid grooves. The viscosity prevents the advancing motion of the three-phase contact line (TPCL), leading to a rapid change in the velocity along the normal direction. This causes an increase in the convexity of the advancing droplet periphery [21]. In the whole process of droplet spreading, it is usually assumed that the initial kinetic energy is mainly consumed by the surface energy and by viscous dissipation [36–39]. The viscous dissipation comes from the attraction force between molecules in the droplets, the adsorption capacity of the solid wall to droplet molecules, and the momentum exchange between droplet flow layers.
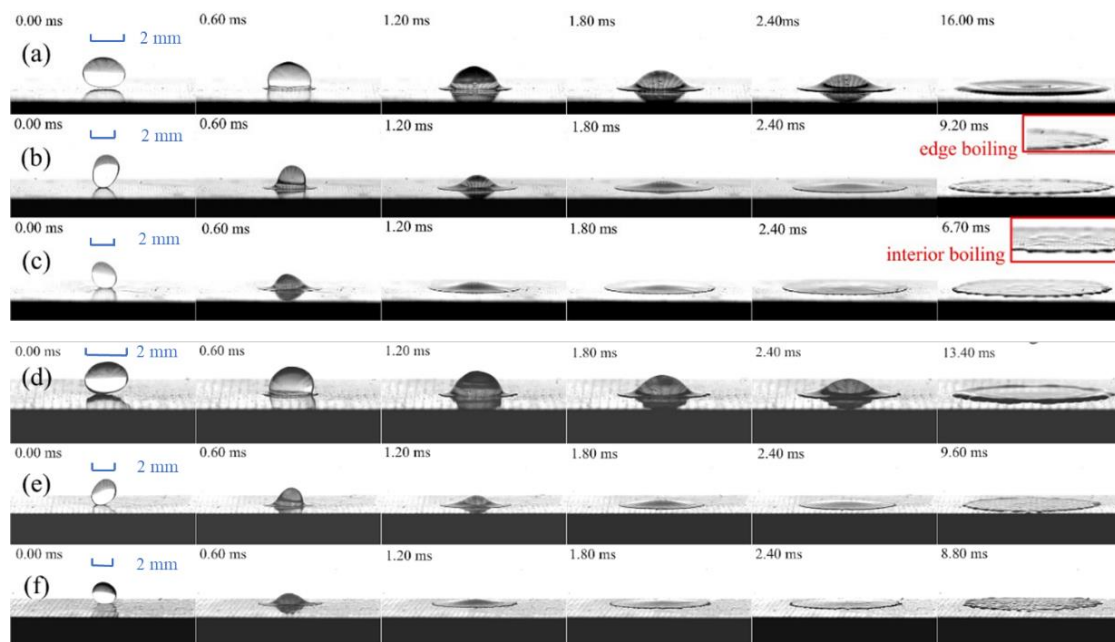
Figure 4. Spreading process of R1336mzz(Z) droplets impinging on low and high roughness surfaces at different *We*. (**a**) *We* = 77, (**b**) *We* = 521 and (**c**) *We* = 948 (*Ra* = 0.8 μm); (**d**) *We* = 81, (**e**) *We* = 543 and (**f**) *We* = 936 (*Ra* = 6.3 μm).

Figure 4b shows the evolution process of droplet morphology under low surface roughness (*Ra* = 0.8m) and medium *We* number case (*We* = 521). The droplet morphology is similar to that at low *We* of 77, but the difference is that the time for droplets to reach the maximum spreading diameter is obviously shortened, and the thickness of the liquid film is thinner when reaching the maximum spreading diameter β_{max} due to the greater spreading kinetic energy of droplet. In addition, "finger-like" disturbance (9.20 ms, Figure 4b) can be observed at the final stage of spreading, which will be discussed in detail in a later section. Different from the low *We*, when β_{max} is reached, the outer edge of the droplet has been boiled and evaporated (9.20 ms, Figure 4b). These phenomena are more obvious under a high *We* number (*We* = 948), as demonstrated in Figure 4c. In addition, when the maximum spreading diameter is reached under a high *We* number, the boiling has propagated from the outer boundary to the inside of the liquid film (6.70 ms, Figure 4c). This can be explained by the fact that the larger kinetic energy at a high *We* number causes the droplets to spread into a thinner and larger liquid film, promoting the heat exchange and evaporation of the liquid film.

At the same time, the dynamic evolution of droplet impinging on high roughness surface of *Ra* = 6.3 μm under low, medium, and high *We* are presented in Figure 4d–f as a comparison. The dynamic behaviors are similar to those under low roughness surfaces. In all the roughness and Weber number ranges studied, no obvious phenomena such as broken splash, recede, rebound, and satellite droplets were observed.

The spreading factor β is able to represent droplet spreading kinetics quantitatively. Figure 5 presents the variations of β with dimensionless time τ under low, medium, and high *We* numbers on different roughness surfaces. As can be seen from this figure, the β-τ curves of different *We* coincide at each roughness in the initial stage of droplet spreading ($\tau < 0.1$), which means that the spreading speed and behavior of droplets at this stage are highly similar. Rioboo et al. [40] believed that the evolution of β was not affected by any factors at the early stage of droplet motion ($\tau < 0.1$). Near $\tau = 0.1$, the β-τ curve of low *We* separates from the curve of medium and high *We*. About $\tau = 1$, the curve of medium *We* separates from the curve of high *We*. In general, a larger *We* results in a faster increase in the spreading factor and a greater slope of the β-τ curve. What is more, with the increase

in *We*, it takes a longer dimensionless time τ for the β-τ curve to approach level and finally form larger β_{max}.
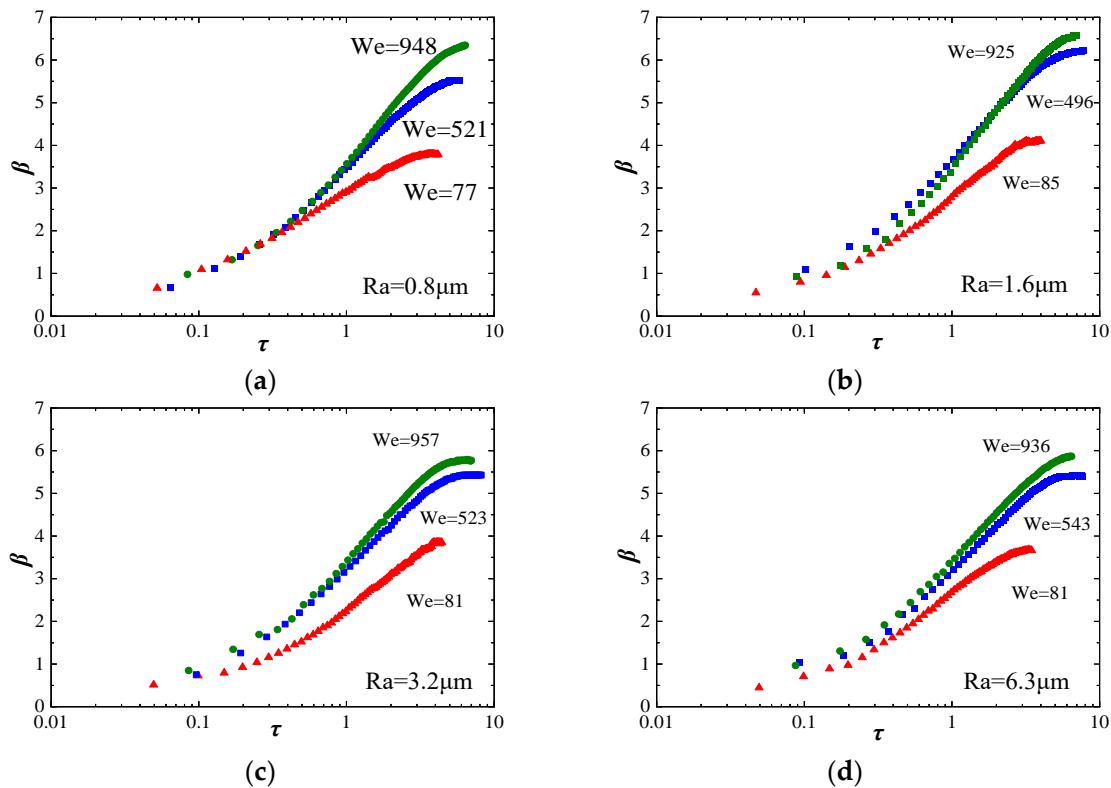

Figure 5. β-τ curves at different *We*. (**a**) *Ra* = 0.8 μm. (**b**) *Ra* = 1.6 μm. (**c**) *Ra* = 3.2 μm. (**d**) *Ra* = 6.3 μm.

3.2. The Influence of Surface Roughness

To explore the influence of roughness on droplet spreading dynamics, this section compares the impact images of droplets on different roughness surfaces at similar *We*, as shown in Figure 6. The outcomes of droplet impingement are similar on four roughness surfaces. No obvious breaking splashes were observed within the range of *We* studied.
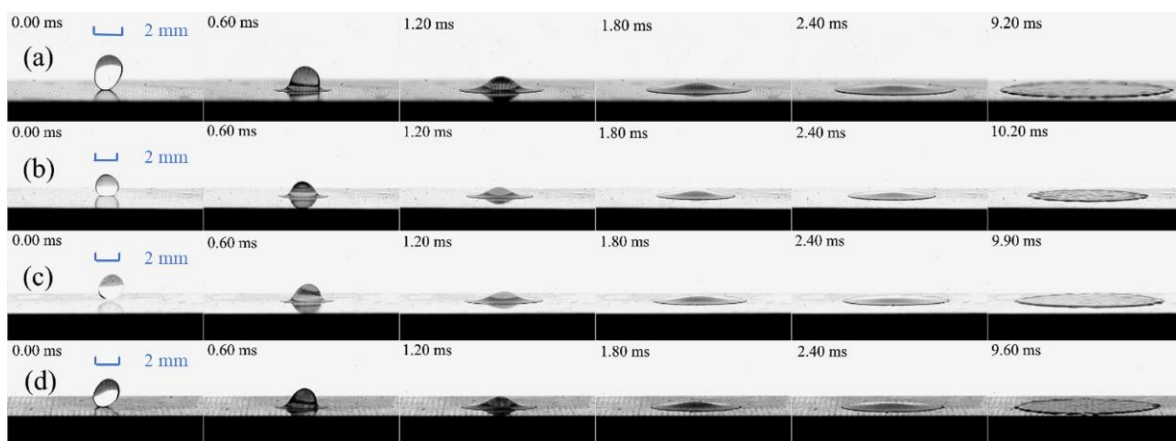

Figure 6. Spreading process of R1336mzz(Z) droplets impinging on different roughness surfaces at medium *We* (*We* ≈ 520). (**a**) *Ra* = 0.8 μm, (**b**) *Ra* = 1.6 μm, (**c**) *Ra* = 3.2 μm and (**d**) *Ra* = 6.3 μm.

Droplet impingement on a groove-textured solid surface may experience one of the following states [21]. (i) Cassie state [41], in which liquid is suspended on the grooves and air is occupied in the valleys of the surface. (ii) Wenzel state [42], in which the liquid impales the valleys. (iii) Intermediate state, in which liquid is partially impaled. When the inertial

force of droplets increases or the surface conditions changes, more liquid will squeeze into the groove gap occupied by air originally, which induces the transition from the Cassie state to the Wenzel state. This transition leads to an increase in the adhesion between the droplet and the wall and high hysteresis in the Wenzel state, making it "sticky" on the textured surface [43]. There are two possible mechanisms for the transition as reported [21,44–46]: sag and de-pinning. Sag means that when the depth of roughness valleys is small enough, the liquid–vapor interface directly contacts the bottom of the valley. In the de-pinning mechanism, when the magnitude of net downward force at TPCL is large enough, the droplet de-pins and causes the liquid to impale the valleys when the depth of roughness valleys increases. Forces acting on the TPCL include droplet impact pressure related to impacting velocity and three interfacial tensions [21].

This study changed the depth of valleys through changing surface roughness. The variable *Ra* is commonly used to reflect the height characteristics of surface microscopic geometry. Figure 7 presents the curves of droplet spreading factors with dimensionless time on different roughness surfaces. Similar phenomena can be observed at three different *We*. The β_{max} first increases with the increase in surface roughness from 0.8 μm to 1.6 μm but decreases obviously with the increase in surface roughness from 1.6 μm to 3.2 μm. When the roughness increases to 6.3 μm, the maximum spreading factors are basically unchanged, but they are always smaller than the β_{max} of the surface with *Ra* = 0.8 μm. The first increase in β_{max} can be explained by the Cassie state. That is, the viscous dissipation is relatively small since the liquid film is suspended on the grooves. As a result, the β_{max} increases with the increase in roughness. With the continued increase in the depth of the grooves, the Cassie–Wenzel transition takes place, leading to a rapid decrease in β_{max} due to the de-pinning mechanism. The partially impaled state between the Cassie state and the Wenzel state consumes part of the energy input to conquer the energy barriers induced by the state transition [47]. What is more, the pinning force at TPCL increases, which leads to an increase in energy dissipation and a significant decrease in the maximum spreading diameter.
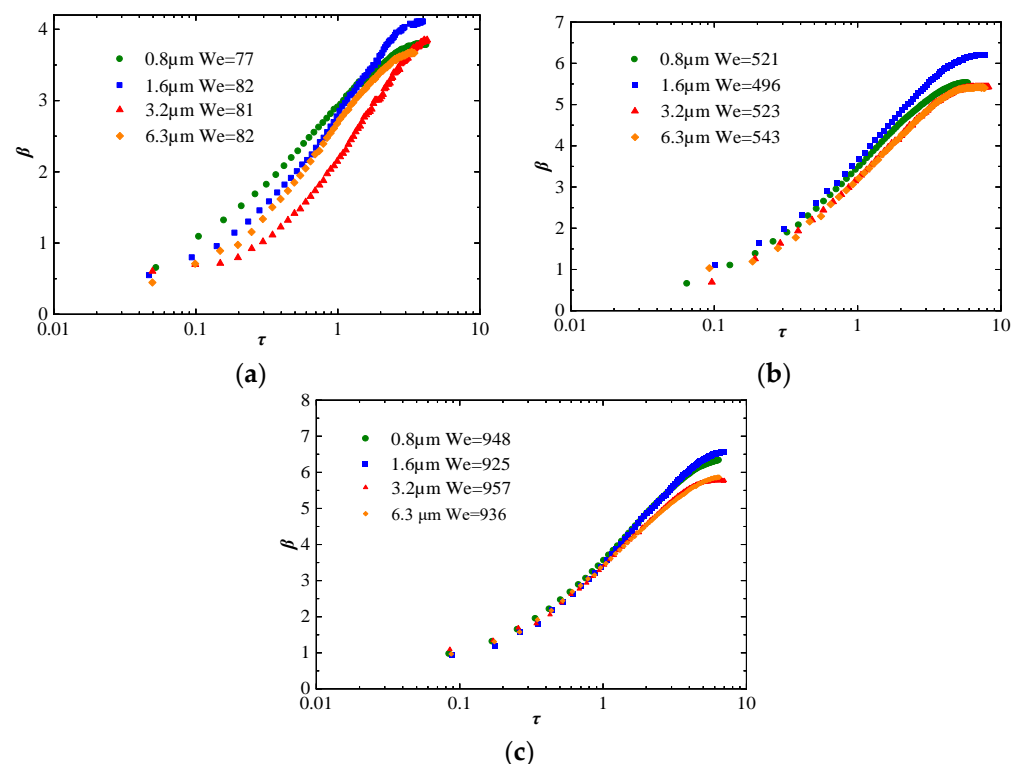

Figure 7. Influence of surface roughness on β-τ curve at three different *We*. (**a**) Low *We*. (**b**) Medium *We*. (**c**) High *We*.

3.3. Finger-like Disturbance Phenomenon

As mentioned above, the "finger-like" disturbance was observed during the droplet spreading process. Droplets do not form regular circles when they spread on solid walls. Instead, some prominent disturbances are formed at the periphery, which have been called "finger" structures in previous studies. There is no unified theory about the formation mechanism of "finger" structures, and some researchers attribute it to the instability caused by the relative motion of the air–liquid interface. Allen [48] suggested that fingers form at the periphery of a droplet because of Rayleigh–Taylor instability, which is caused by the acceleration of the interface between two kinds of fluid with different densities. In addition, surface roughness also has a certain influence. Stow and Hadfield [49] put forward that the surface roughness caused the instability of the liquid film, thus affecting the splash phenomenon because the "finger" disturbance formed the necessary condition for the splash. However, due to the differences in hydrophilicity, surface structure, and droplet properties, the shape and number of "finger-like" disturbances in this paper are different from those of previous studies.

The "finger disturbance" observed in this study is weak but has more waves. To eliminate the influence of different initial diameters on the number of fingers, the number of fingers following refers to the total number of fingers at the maximum diameter divided by initial diameters, that is, the number in a unit circumference of a droplet. Figure 8 shows the relationship between the number of "fingers" and impact velocity on different roughness surfaces. It can be inferred that roughness has little effect on the number and shape of the "finger" disturbance, but impact velocity mainly determines the finger number. This finding is consistent with that of Aziz and Chandra [36]. R-Square testing was used to explore the relationship between finger number and impact velocity. The R-Square value on four roughness surfaces are 0.838, 0.922, 0.876, and 0.948 in turn, and it is concluded that the number of fingers presents almost linear variation with the impact velocity.
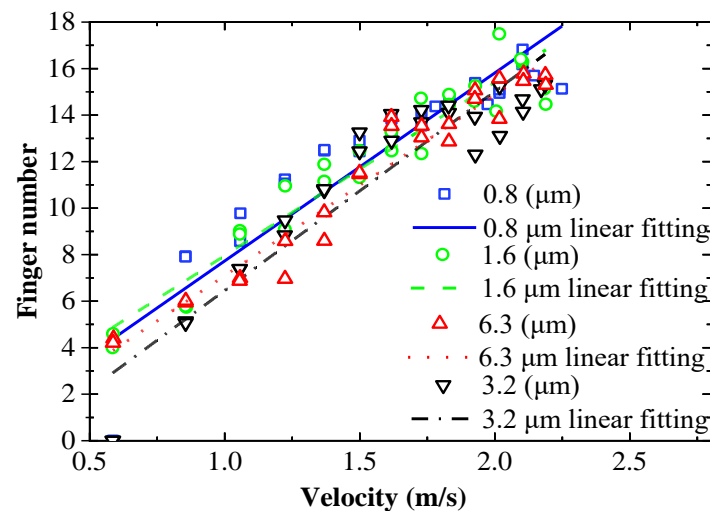

Figure 8. Variation of "finger" numbers with impact velocity.

3.4. Empirical Formula of β_{max}

The β_{max} of droplets impingement is one of the most important parameters of droplet impact dynamics, which directly represents the spreading ability of droplets under different working conditions. Studying β_{max} has many applications in inkjet printing, spray cooling, and other fields. The maximum spreading factor β_{max} is closely related to *We* and *Re* numbers, as demonstrated by previous studies. Pasandideh–Fard et al. [37] proposed a model to describe the variation of β_{max} with *We* and *Re* based on energy conservation of kinetic energy, surface energy, and viscous dissipation, considering droplets at maximum spreading diameter as cylindrical geometry. Compared with experimental data, the model showed a mean error of 8.70%. Roisman and Ilia [50] proposed a semi-empirical model

considering the flow within the impacting droplet and showed the largest mean error of 14.64%. Scheller and Bousfifield (1995) [51] proposed an empirical formula based on regression analysis where the mean error is 14.33%. Seo et al. [14] found that existing models did not perform well for low-viscous liquids and modified the Scheller and Bousfifield model by changing its coefficients, which showed better agreement with different liquids.

　　Figure 9 shows the experimental data of $\beta_{\max}$ falling from different heights on the surface with Ra = 0.8 μm and the comparison with the data predicted by the different models mentioned above. Seo's model shows the smallest error (6.81%) for low-viscous R1336mzz(Z) impingement. However, to improve the predictive capability further, a new empirical model based on Scheller and Bousfifield's regression analysis has been proposed in this study, as expressed in equation (6), adopting the method of Seo et al. Table 2 summaries the predictive performance of different models. Our new empirical model has the smallest mean error (5.53%) for the prediction of $\beta_{\max}$ in R1336mzz(Z) impingement. To further examine the sensitivity of the new model on the surface roughness, Figure 10 plots the experimental data of $\beta_{\max}$ and the predictive curve by the new model based on regression analysis under four roughness surfaces. In general, the predicting curve by this model is able to represent $\beta_{\max}$ variation in practice reasonably.

$$\beta_{\max} = 0.923 \left(\frac{We}{Oh} \right)^{0.143} \tag{7}$$
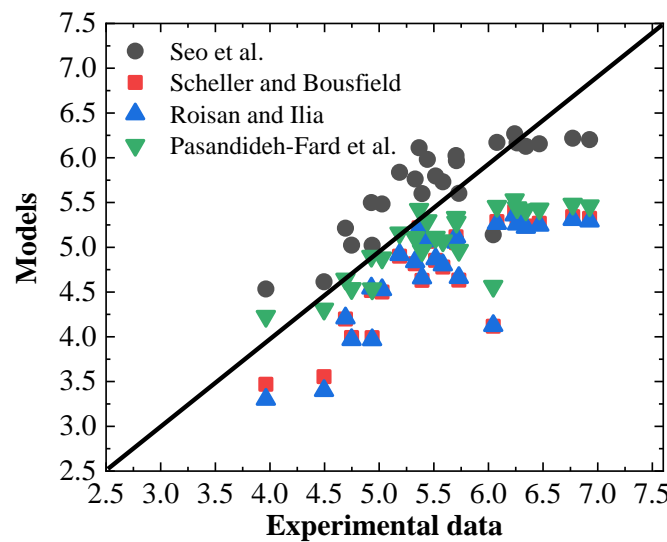

Figure 9. Comparison of experimental data with the predictive data by previous models.

Table 2. Summary of models and their predictive mean errors.

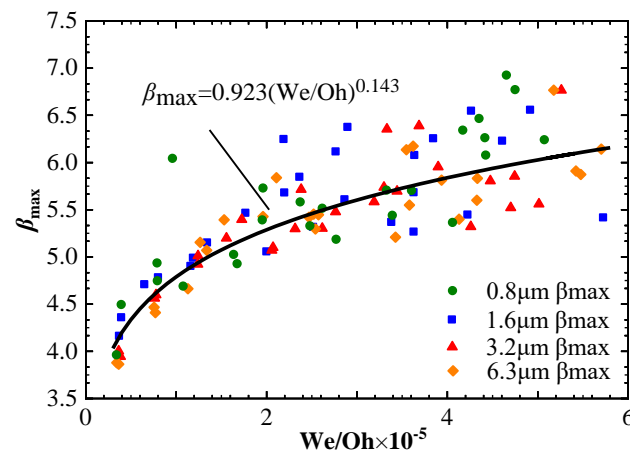| Model	Expression	Mean-Error (%)
Pasandideh–Fard et al. [37]	$\beta_{\max} = \sqrt{\dfrac{We + 12}{3(1 - \cos\theta) + 4\left(\frac{We}{\sqrt{Re}}\right)}}$	8.70
Roisman and Ilia [50]	$\beta_{\max} = \left(0.87 Re^{\frac{1}{5}} - 0.4 Re^{\frac{2}{5}} We^{-\frac{1}{2}} \right)$	14.64
Scheller and Bousfield [51]	$\beta_{\max} = 0.61 \left(\frac{We}{Oh} \right)^{0.166}$	14.33
Seo et al. [14]	$\beta_{\max} = 1.27 \left(\frac{We}{Oh} \right)^{0.122}$	6.81
New empirical model	$\beta_{\max} = 0.923 \left(\frac{We}{Oh} \right)^{0.143}$	5.53

Figure 10. Experimental data and model prediction of β_{max} by the new empirical formula of droplet impinging on four different roughness surfaces.

4. Conclusions

In this paper, an experimental system for single droplet generation and impingement with low-boiling point refrigerant under atmospheric pressure has been constructed successfully to investigate the dynamic behavior of R1336mzz(Z) droplet impinging on the solid surface of carbon steel 45. The effects of roughness (0.8 μm, 1.6 μm, 3.2 μm, 6.3 μm) and *We* (50–1000) on droplet impinging dynamics are explored. The main conclusions are summarized as follows:

(1) The shape of the droplet changed from a truncated spherical shape to a thin liquid layer and then spread into a liquid film with a thicker rim during the impinging period. Moreover, boiling and "finger disturbance" were observed. Boiling was noticed to be more obvious under higher *We*.

(2) *We* had a significant effect on the dynamic behavior of droplet spreading. When $0 < \tau < 0.1$, the β-τ curves almost coincided. At $\tau = 0.1$, the curves of low *We* had a lower slope and were separated from those of medium and high *We*. At about $\tau = 1$, the curves at medium *We* separated from the curve at high *We* number. With the increase in *We*, the curve slope became larger, and τ to reach β_{max} became longer.

(3) The droplet exhibited the Cassie state on the surface with low roughness, and β_{max} increased with the increase in roughness. At a certain threshold of *Ra* between 1.6 μm and 3.2 μm, the droplet underwent a Cassie–Wenzel transition, and β_{max} was significantly reduced due to larger energy dissipation.

(4) The empirical formula of β_{max} on the carbon steel walls was proposed based on the regression analysis. The formula fitted well with experimental data on solid surfaces with different roughness.

Author Contributions: Conceptualization, Z.-F.Z. and S.-Y.C.; methodology, D.-Q.Z.; software, H.-J.X.; validation, B.C. and Q.Z.; formal analysis, H.-J.X.; investigation, S.-Y.C. and Q.Z.; data curation, S.-Y.C.; writing—original draft preparation, S.-Y.C.; writing—review and editing, Z.-F.Z.; visualization, D.-Q.Z.; supervision, Z.-F.Z. and B.C.; project administration, Z.-F.Z.; funding acquisition, Z.-F.Z. All authors have read and agreed to the published version of the manuscript.

Institutional Review Board Statement: Not applicable.

Informed Consent Statement: Not applicable.

Data Availability Statement: The data presented in this study are available on request from the corresponding author.

Conflicts of Interest: The authors declare no conflict of interest.

References

1. Miao, J.; He, S.; Lu, Y.; Wu, Y.; Wu, X.; Zhang, G.; Gao, M.; Geng, Z.; Zhang, S. Comparison on cooling performance of pre-cooled natural draft dry cooling towers using nozzles spray and wet medium. *Case Stud. Therm. Eng.* **2021**, *27*, 101274. [CrossRef]
2. Benther, J.D.; Pelaez-Restrepo, J.D.; Stanley, C.; Rosengarten, G. Heat transfer during multiple droplet impingement and spray cooling: Review and prospects for enhanced surfaces. *Int. J. Heat Mass Transf.* **2021**, *178*, 121587. [CrossRef]
3. Xu, R.; Wang, G.; Jiang, P. Spray Cooling on Enhanced Surfaces: A Review of the Progress and Mechanisms. *J. Electron. Packag.* **2021**, *144*, 010802. [CrossRef]
4. Zhao, Y.; Gong, S.; Zhang, C.; Ge, M.; Xie, L. Performance analysis of a solar photovoltaic power generation system with spray cooling. *Case Stud. Therm. Eng.* **2022**, *29*, 101723. [CrossRef]
5. Cheng, W.-L.; Zhang, W.-W.; Chen, H.; Hu, L. Spray cooling and flash evaporation cooling: The current development and application. *Renew. Sustain. Energy Rev.* **2016**, *55*, 614–628. [CrossRef]
6. Zhou, Z.-F.; Lin, Y.-K.; Tang, H.-L.; Fang, Y.; Chen, B.; Wang, Y.-C. Heat transfer enhancement due to surface modification in the close-loop R410A flash evaporation spray cooling. *Int. J. Heat Mass Transf.* **2019**, *139*, 1047–1055. [CrossRef]
7. Wang, R.; Zhou, Z.F.; Chen, B.; Bai, F.L.; Wang, G.X. Surface heat transfer characteristics of R404A pulsed spray cooling with an expansion-chambered nozzle for laser dermatology. *Int. J. Refrig.* **2015**, *60*, 206–216. [CrossRef]
8. Nelson, J.S. Dynamic Epidermal Cooling During Pulsed Laser Treatment of Port-Wine Stain. *Arch Derm.* **1995**, *131*, 695–700. [CrossRef]
9. Worthington, A.M. A Second Paper on the Forms Assumed by Drops of Liquids Falling Vertically on a Horizontal Plate. *Proc. R. Soc. Lond.* **1876**, *25*, 261–272.
10. Rioboo, R.; Tropea, C.; Marengo, M. Outcomes from a drop impact on solid surfaces. *At. Sprays* **2001**, *11*, 12. [CrossRef]
11. Chen, L.; Li, Z. Bouncing droplets on nonsuperhydrophobic surfaces. *Phys. Rev. E Stat. Nonlinear Soft Matter Phys.* **2010**, *82*, 016308. [CrossRef]
12. Bhardwaj, R.; Attinger, D. Non-isothermal wetting during impact of millimeter size water drop on a flat substrate: Numerical investigation and comparison with high-speed visualization experiments. *Int. J. Heat Fluid Flow* **2008**, *29*, 1422–1435. [CrossRef]
13. Bange, P.G.; Patil, N.D.; Bhardwaj, R. Impact Dynamics of a Droplet on a Heated Surface. In Proceedings of the International Conference of Fluid Flow, Heat and Mass Transfer, Niagara Falls, ON, Canada, 7–9 June 2018.
14. Seo, J.; Lee, J.S.; Kim, H.Y.; Yoon, S.S. Empirical model for the maximum spreading diameter of low-viscosity droplets on a dry wall. *Exp. Therm. Fluid Sci.* **2015**, *61*, 121–129. [CrossRef]
15. Tian, J.M.; Chen, B. Dynamic behavior of non-evaporative droplet impact on a solid surface: Comparative study of R113, water, ethanol and acetone. *Exp. Therm. Fluid Sci.* **2019**, *105*, 153–164. [CrossRef]
16. Xu, L.; Zhang, W.W.; Nagel, S.R. Drop Splashing on a Dry Smooth Surface. *Phys. Rev. Lett.* **2005**, *94*, 184505. [CrossRef]
17. Range, K.; Feuillebois, F. Influence of Surface Roughness on Liquid Drop Impact. *J. Colloid Interface Sci.* **1998**, *203*, 16–30. [CrossRef]
18. Tang, C.L.; Qin, M.X.; Weng, X.Y.; Zhang, X.H.; Zhang, P.; Li, J.L.; Huang, Z.H. Dynamics of droplet impact on solid surface with different roughness—ScienceDirect. *Int. J. Multiph. Flow* **2017**, *96*, 56–69. [CrossRef]
19. Kuhn, C.; Schweigert, D.; Kuntz, C.; Brnhorst, M. Single droplet impingement of urea water solution on heated porous surfaces. *Int. J. Heat Mass Transf.* **2021**, *181*, 121836. [CrossRef]
20. Vaikuntanathan, V.; Sivakumar, D. Maximum Spreading of Liquid Drops Impacting on Groove-Textured Surfaces: Effect of Surface Texture. *Langmuir ACS J. Surf. Colloids* **2016**, *32*, 2399–2409. [CrossRef]
21. Vaikuntanathan, V.; Sivakumar, D. Transition from Cassie to impaled state during drop impact on groove-textured solid surfaces. *Soft Matter* **2014**, *10*, 2991–3002. [CrossRef]
22. Lee, M.; Chang, Y.S.; Kim, H.-Y. Drop impact on microwetting patterned surfaces. *Phys. Fluids* **2010**, *22*, 072101. [CrossRef]
23. Moon, J.H.; Cho, M.; Lee, S.H. Dynamic contact angle and liquid displacement of a droplet imping on heated textured surfaces—ScienceDirect. *Exp. Therm. Fluid Sci.* **2019**, *101*, 128–135. [CrossRef]
24. Ogata, S.; Nakanishi, R. Effect of Surface Textures and Wettability on Droplet Impact on a Heated Surface. *Processes* **2021**, *9*, 350. [CrossRef]
25. Lv, C.; Hao, P.; Zhang, X.; He, F. Drop impact upon superhydrophobic surfaces with regular and hierarchical roughness. *Appl. Phys. Lett.* **2016**, *108*, 141602. [CrossRef]
26. Zhang, R.; Zhang, X.; Hao, P.; He, F. Internal rupture and rapid bouncing of impacting drops induced by submillimeter-scale textures. *Phys. Rev. E* **2017**, *95*, 063104. [CrossRef]
27. Liu, J. *Droplet Impact Dynamics and Related Heat Transfer Phenomena*; University of California: Riverside, CA, USA, 2008.
28. Liu, J.; Franco, W.; Aguilar, G. The Effect of Roughness on the Impact Dynamics and Heat Transfer of Cryogen Droplets Impinging Onto Indented Skin Phantoms. In Proceedings of the ASME 2005 Summer Heat Transfer Conference collocated with the ASME 2005 Pacific Rim Technical Conference and Exhibition on Integration and Packaging of MEMS, NEMS, and Electronic Systems, San Francisco, CA, USA, 17–22 July 2005; pp. 861–866.

29. Liu, J.; Franco, W.; Aguilar, G. Effect of Surface Roughness on Single Cryogen Droplet Spreading. *J. Fluids Eng.* **2008**, *130*, 041402. [CrossRef]

30. Zhang, Z.; Li, Q.; Hu, D. Experimental investigation on heat transfer characteristics of R1336mzz flash spray cooling. *Appl. Therm. Eng.* **2020**, *174*, 115277. [CrossRef]

31. Fabian, D.; Jonas, F.; Florian, K.; Christopher, S.; Sebastian, E.; Christoph, W.; Hartmut, S. R1224yd(Z), R1233zd(E) and R1336mzz(Z) as replacements for R245fa: Experimental performance, interaction with lubricants and environmental impact. *Appl. Energy* **2021**, *288*, 116661.

32. Kedzierski, M.A.; Lin, L. Pool boiling of HFO-1336mzz(Z) on a reentrant cavity surface—ScienceDirect. *Int. J. Refrig.* **2019**, *104*, 476–483. [CrossRef]

33. Sun, Y.; Li, X.; Meng, X.; Wu, J. Measurement and Correlation of the Liquid Density and Viscosity of HFO-1336mzz(Z) (cis-1,1,1,4,4,4-Hexafluoro-2-butene) at High Pressure. *J. Chem. Eng. Data* **2018**, *64*, 395–403. [CrossRef]

34. Harkins, W.D.; Brown, F.E. The determination of surface tension (free surface energy), and the weight of falling drops: The surface tension of water and benzene by the capillary height method. *J. Am. Chem. Soc* **1919**, *41*, 499–524. [CrossRef]

35. Josserand, C.; Lemoyne, L.; Troeger, R.; Zaleski, S. Droplet impact on a dry surface: Triggering the splash with a small obstacle. *J. Fluid Mech.* **2005**, *524*, 47–56. [CrossRef]

36. Aziz, S.D.; Chandra, S. Impact, recoil and splashing of molten metal droplets. *Int. J. Heat Mass Transf.* **2000**, *43*, 2841–2857. [CrossRef]

37. Pasandideh-Fard, M.; Qiao, Y.M.; Chandra, S.; Mostaghimi, J. Capillary Effects during Droplet Impact on a Solid Surface. *Phys. Fluids* **1996**, *8*, 650–659. [CrossRef]

38. Ukiwe, C.; Kwok, D.Y. On the maximum spreading diameter of impacting droplets on well-prepared solid surfaces. *Langmuir ACS J. Surf. Colloids* **2005**, *21*, 666–673. [CrossRef]

39. Wildeman, S.; Visser, C.W.; Chao, S.; Lohse, D. On the spreading of impacting drops. *J. Fluid Mech.* **2017**, *805*, 636–655. [CrossRef]

40. Rioboo, R.; Marengo, M.; Tropea, C. Time evolution of liquid drop impact onto solid, dry surfaces. *Exp. Fluids* **2002**, *33*, 112–124. [CrossRef]

41. Cassie, A.B.D.; Baxter, S. Wettability of porous surfaces. *Trans. Faraday Soc.* **1944**, *40*, 546–551. [CrossRef]

42. Wenzel, R.N. Resistance of solid surfaces to wetting by water. *Trans. Faraday Soc.* **1936**, *28*, 988–994. [CrossRef]

43. Bo, H.; Lee, J.; Patankar, N.A. Contact angle hysteresis on rough hydrophobic surfaces. *Colloids Surf. A Physicochem. Eng. Asp.* **2016**, *248*, 101–104.

44. Bartolo, D.; Bouamrirene, F.; Verneuil, É.; Buguin, A.; Silberzan, P.; Moulinet, S. Bouncing or sticky droplets: Impalement transitions on superhydrophobic micropatterned surfaces. *EPL (Europhys. Lett.)* **2006**, *74*, 299. [CrossRef]

45. Deng, T.; Varanasi, K.K.; Ming, H.; Bhate, N.; Blohm, M. Nonwetting of impinging droplets on textured surfaces. *Appl. Phys. Lett.* **2009**, *94*, 481. [CrossRef]

46. Rioboo, R.; Voue, M.; Vaillant, A.; Coninck, J.D. Drop impact on porous superhydrophobic polymer surfaces. *Langmuir ACS J. Surf. Colloids* **2008**, *24*, 14074–14077. [CrossRef] [PubMed]

47. Bormashenko, E. Progress in understanding wetting transitions on rough surfaces. *Adv. Colloid Interface Sci.* **2015**, *222*, 92–103. [CrossRef]

48. Allen, R.F. The role of surface tension in splashing. *J. Colloid Interface Sci.* **1975**, *51*, 350–351. [CrossRef]

49. Stow, C.D.; Hadfield, M.G. An Experimental Investigation of Fluid Flow Resulting from the Impact of a Water Drop with an Unyielding Dry Surface. *Proc. R. Soc. A Math.* **1981**, *373*, 419–441.

50. Roisman, I.V. Inertia dominated drop collisions. II. An analytical solution of the Navier–Stokes equations for a spreading viscous film. *Phys. Fluids* **2009**, *21*, 296. [CrossRef]

51. Scheller, B.L.; Bousfield, D.W. Newtonian drop impact with a solid surface. *Aiche J.* **2010**, *41*, 1357–1367. [CrossRef]